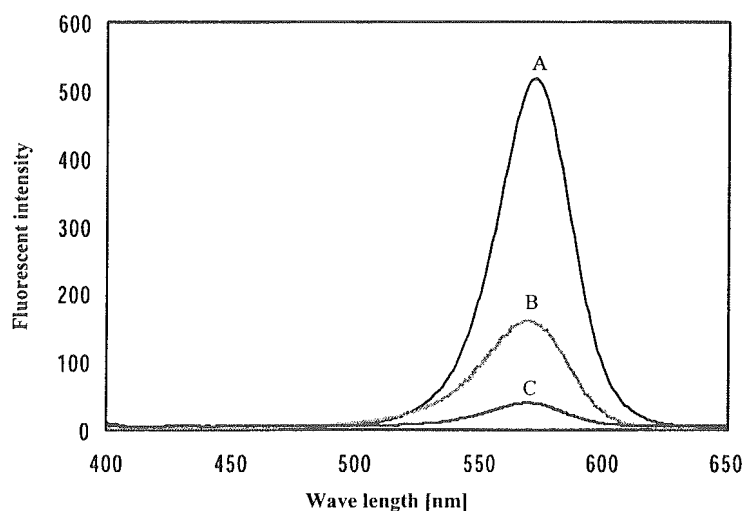


**Table 2** Stability of each quantum dot for acid, salts, base, and buffer

	QD-SO <sub>3</sub> <sup>-</sup>		QD-SO <sub>3</sub> -SSA		QD-MUA		QD-MUA-SSA		QD-NH <sub>2</sub>	
	1 h	o/n	1 h	o/n	1 h	o/n	1 h	o/n	1 h	o/n
Water	+	+	+	+	+	+	+	+	+	-
0.25 mM H <sub>2</sub> SO <sub>4</sub> /pH 3.2	+	-	+	+	q	q	+	-	q	q
0.1 mM H <sub>2</sub> SO <sub>4</sub> /pH 3.7	+	+	+	+	q	q	+	+	+	-
0.01 mM H <sub>2</sub> SO <sub>4</sub> /pH 4.6	+	+	+	+	+	+	+	+	+	-
Borate buffer/pH 9	+	+	+	+	+	-	+	+	+	+
1 M NaCl	+	+	+	+	-	-	+	-	-	-
5 M NaCl	+	+	+	+	-	-	+	-	q	q
PBS	+	+	+	+	-	-	+	-	-	-
MEM	+	+	+	+	-	-	+	+	+	-

+: dispersion, -: aggregation, q: quenching

Stabilities of each quantum dot for acid, salts, base, and buffer solutions were measured with 0.1 mg/mL of concentration of each quantum dot. And photos were taken after 1 h and overnight. o/n shows after overnight.



**Fig. 2** Emission spectra of each quantum dot. Spectra A stands for QD-MUA, spectra B and spectra C stand for QD-SO<sub>3</sub><sup>-</sup> and QD-NH<sub>2</sub> respectively. Each quantum dot was dissolved in distilled water and their emission spectra were measured with FP-6500. Each quantum dot was excited at 350 nm. Concentration of each quantum dot was 0.1 mg/mL

of  $19.97 \pm 6.563$  nm. The diameter of the rest is  $572 \pm 418$  nm but these particles probably aggregated in water. The diameter of QD-NH<sub>2</sub> is  $10.36 \pm 3.224$  nm, which is almost the same size as that of QD-SO<sub>3</sub><sup>-</sup>. The zeta potentials of QD-SO<sub>3</sub><sup>-</sup>, QD-MUA and QD-NH<sub>2</sub> were  $-32.7$ ,  $-32.3$ , and  $+10.95$  mV, respectively. The results of these measurements were consistent with what we can predict from the structure of each quantum dot.

## 2.2 Stability in acid, salts, base, and buffer solution

The results about the stability of the quantum dots are summarized in **Table 2**. Here, the stability stands for the condition that quantum dots disperse and give off light in the solutions in this study. In acid, salt, and buffer solutions, the non-coat QD-SO<sub>3</sub><sup>-</sup> is stable except the case of pH 3.2 after 24-h incubation. The SSA-

coated QD-SO<sub>3</sub><sup>-</sup> is always stable in all the solutions. The stability of the non-coated QD-MUA was quite low and quenching was occurred in acid (see **Figure 3**). The SSA-coated QD-MUA was stable under all the acidic conditions after 1-h incubation and in NaCl solutions as well in this experiment, but it aggregates at pH 3.2 and NaCl solutions after 24 h. The QD-NH<sub>2</sub> generally was not stable in all the solutions after 24 h.

## 3. Discussion

Our study is based on the prediction that QD-SO<sub>3</sub><sup>-</sup> shows high stability in low pH solutions because this surface ligand is expected to be compatible with the sulfuric acid. Thus, let us compare the stability of QD-SO<sub>3</sub><sup>-</sup>, QD-MUA and QD-NH<sub>2</sub> in detail.

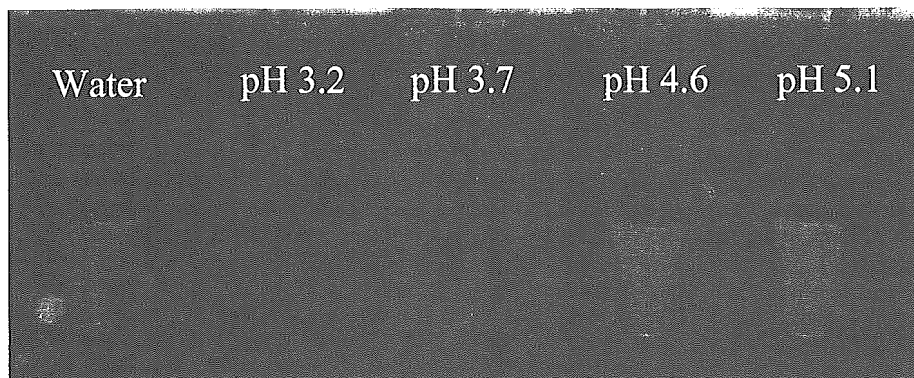


**Fig. 3** Representative results of QD-MUA. Photos were taken after 24 h. The pictures stand for QD-MUA in water, acidic solutions of pH 3.2, 3.7, 4.6 and 5.1 from the left-hand side, respectively

Firstly, we compare the stability of the quantum dots without the SSA coating. Under acidic conditions, the QD-SO<sub>3</sub><sup>-</sup> is more stable than the QD-MUA (see the second and third rows in Table 2). The QD-MUA undergoes quenching under the acidic conditions, pH 3.2 and pH 3.7. There are several possibilities for the reasons of the quenching: (1) the surface states of the quantum dots are changed by the acidic solvent; (2) the exciting energy is transformed to energy other than fluorescence; and (3) the ZnS shell of the quantum dot is destroyed by the acidic solvent. Among them, the last possibility is the most plausible because the quenching occurred rapidly when the quantum dots was added into the solvent. This quenching results from the fact that the sulfonyl group of QD-SO<sub>3</sub><sup>-</sup> is more compatible with the sulfuric acid than the carboxyl group of the QD-MUA and the ZnS shell of the QD-SO<sub>3</sub><sup>-</sup> can be protected. In addition, the hydrophobic alkyl group in the ligand of QD-MUA is longer than that of QD-SO<sub>3</sub><sup>-</sup> so that the ligands might prevent each other from bonding to the surface of the quantum dot during the synthesis process. As a result, the number of surface ligands of the QD-MUA is smaller than that of the QD-SO<sub>3</sub><sup>-</sup>, and the ZnS shell is easily attacked by the acidic molecules.

Also in the buffer and salt solutions, the non-coated QD-SO<sub>3</sub><sup>-</sup> is more stable than the non-coated QD-MUA (see the fifth to ninth rows in Table 2). This is because the ionization of the sulfonyl group of the QD-SO<sub>3</sub><sup>-</sup> is larger than the carboxyl group of the QD-MUA. Accordingly, the surface of QD-SO<sub>3</sub><sup>-</sup> is not easily terminated by hydrogen and the polarity of the QD-SO<sub>3</sub><sup>-</sup> can be kept in the buffer and salt solutions.

Secondly, we compare the SSA-coated and non-coated quantum dots and discuss the effect of the SSA coating. While Hanaki *et al.* (2003) have already reported that SSA raises the dispersibility of QD-MUA in MEM (see the last row in Table 2), we found that the same effect can be observed for the SSA-coated QD-MUA in acid and borate buffer as well. This result

indicates that the SSA coating the surface of the quantum dots prevents the contact of the quantum dots each other, regardless of the kind of solvents. On the contrary, it is noteworthy that there is no remarkable difference between the SSA-coated QD-SO<sub>3</sub><sup>-</sup> and non-coated QD-SO<sub>3</sub><sup>-</sup>. For the QD-SO<sub>3</sub><sup>-</sup>, SSA coating has no significant effect for the stability in acid, buffer, and salt solutions. This result implies that the QD-SO<sub>3</sub><sup>-</sup> has a great advantage over the QD-MUA as for dispersion in solutions.

For industrial applications, SSA coating is not always needed because additional processes of the surface coating take one's time and the SSA must be denatured at high temperature. Concerning this point, the QD-SO<sub>3</sub><sup>-</sup> coated with SSA has an important meaning for biological applications. The SSA coating has significant roles of carrying the quantum dots into cells, and without coating, they do not get inside cells (data not shown).

Finally, we mention an advantageous property of the QD-SO<sub>3</sub><sup>-</sup>. The QD-SO<sub>3</sub><sup>-</sup> has smaller particle size than the QD-MUA: the diameter of the QD-SO<sub>3</sub><sup>-</sup> is about a half compared to QD-MUA. This means that the QD-SO<sub>3</sub><sup>-</sup> is more suitable for the use in immunostaining.

It is desirable for industrial applications to determine the threshold of the stability against acids. For this purpose, the titration is a better way to give their exact values. We are about to perform such experiments in the future work.

#### Acknowledgment

We thank Dr. Richard Tilley at Victoria University in Wellington and Hideki Maruyama at Shionogi & Co., Ltd. for the important discussion and help. We were supported by Grants-in-Aid for the Advancement of Medical Equipment of the Ministry of Health, Labor and Welfare and Japan Association.

#### Literature Cited

Åkerman, M. E., W. C. W. Chan, P. Laakkonen, S. N. Bhatia and E. Ruoslahti; "Nanocrystal Targeting *in vivo*," *Proc. Natl. Acad. Sci. U.S.A.*, **99**, 12617–12621 (2002)

- Alivisatos, P.; "The Use of Nanocrystals in Biological Detection," *Nat. Biotechnol.*, **22**, 47–52 (2004)
- Chan, W. C. W. and S. Nie; "Quantum Dot Bioconjugates for Ultrasensitive Nonisotopic Detection," *Science*, **281**, 2016–2018 (1998)
- Clapp, A. R., I. L. Medintz, J. M. Mauro, B. R. Fisher, M. G. Bawendi and H. Mattoussi; "Fluorescence Resonance Energy Transfer between Quantum Dot Donors and Dye-Labeled Protein Acceptors," *J. Am. Chem. Soc.*, **126**, 301–310 (2004)
- Coe, S., W.-K. Woo, M. Bawendi and V. Bulovič; "Electroluminescence from Single Monolayers of Nanocrystals in Molecular Organic Devices," *Nature*, **420**, 800–802 (2002)
- Dubertret, B., P. Skourides, D. J. Norris, V. Noireaux, A. H. Brivanlou and A. Libchaber; "In vivo Imaging of Quantum Dots Encapsulated in Phospholipid Micelles," *Science*, **298**, 1759–1762 (2002)
- Gao, X., Y. Cui, R. M. Levenson, L. W. K. Chung and S. Nie; "In vivo Cancer Targeting and Imaging with Semiconductor Quantum Dots," *Nat. Biotechnol.*, **22**, 969–976 (2004)
- Han, M., X. Gao, J. Z. Su and S. Nie; "Quantum-Dot-Tagged Microbeads for Multiplexed Optical Coding of Biomolecules," *Nat. Biotechnol.*, **19**, 631–635 (2001)
- Hanaki, K., A. Momo, T. Oku, A. Komoto, S. Maenosono, Y. Yamaguchi and K. Yamamoto; "Semiconductor Quantum Dot/Albumin Complex Is a Long-Life and Highly Photostable Endosome Marker," *Biochem. Biophys. Res. Co.*, **302**, 496–501 (2003)
- Hines, M. A. and P. Guyot-Sionnest; "Synthesis and Characterization of Strongly Luminescing ZnS-Capped CdSe Nanocrystals," *J. Phys. Chem.*, **100**, 468–471 (1996)
- Hoshino, A., K. Hanaki, K. Suzuki and K. Yamamoto; "Applications of T-Lymphoma Labeled with Fluorescent Quantum Dots to Cell Tracing Markers in Mouse Body," *Biochem. Biophys. Res. Co.*, **314**, 46–53 (2004)
- Huang, P., P. L. Olive and R. E. Durand; "Use of the Comet Assay for Assessment of Drug Resistance and Its Modulation *in vivo*," *British Journal of Cancer*, **77**, 412–416 (1998)
- Jaffar, S., K. T. Nam, A. Khademhosseini, J. Xing, R. S. Langer and A. M. Belcher; "Layer-by-Layer Surface Modification and Patterned Electrostatic Deposition of Quantum Dots," *Nano Lett.*, **4**, 1421–1425 (2004)
- Li, X., Y. Wu, D. Steel, D. Gammon, T. H. Stievater, D. S. Katzer, D. Park, C. Piermarocchi and L. J. Sham; "An All-Optical Quantum Gate in a Semiconductor Quantum Dot," *Science*, **301**, 809–811 (2003)
- Mattoussi, H., J. M. Mauro, E. R. Goldman, G. P. Anderson, V. C. Sundar, F. V. Mikulec and M. G. Bawendi; "Self-Assembly of CdSe-ZnS Quantum Dot Bioconjugates Using an Engineered Recombinant Protein," *J. Am. Chem. Soc.*, **122**, 12142–12150 (2000)
- Murray, C. B., D. J. Norris and M. G. Bawendi; "Synthesis and Characterization of Nearly Monodisperse CdE (E = Sulfur, Selenium, Tellurium) Semiconductor Nanocrystallites," *J. Am. Chem. Soc.*, **115**, 8706–8715 (1993)
- Peng, X., M. C. Schlamp, A. V. Kadavanich and A. P. Alivisatos; "Epitaxial Growth of Highly Luminescent CdSe/CdS Core/Shell Nanocrystals with Photostability and Electronic Accessibility," *J. Am. Chem. Soc.*, **119**, 7019–7029 (1997)
- Santori, C., D. Fattal, J. Vučkovič, G. S. Solomon and Y. Yamamoto; "Indistinguishable Photons from a Single-Photon Device," *Nature*, **419**, 594–597 (2002)
- Santra, S., H. Yang, P. H. Holloway, J. T. Stanley and R. A. Mericle; "Synthesis of Water-Dispersible Fluorescent, Radio-Opaque, and Paramagnetic CdS:Mn/ZnS Quantum Dots: A Multifunctional Probe for Bioimaging," *J. Am. Chem. Soc.*, **127**, 1656–1657 (2005)
- Shiohara, A., A. Hoshino, K. Hanaki, K. Suzuki and K. Yamamoto; "On the Cyto-Toxicity Caused by Quantum Dots," *Microbiol. Immunol.*, **48**, 669–675 (2004)
- Unold, T., K. Mueller, C. Lienau, T. Elsaesser and A. D. Wieck; "Optical Stark Effect in a Quantum Dot: Ultrafast Control of Single Exciton Polarizations," *Phys. Rev. Lett.*, **92**, 157401 (2004)
- Weig, E. M., R. H. Blick, T. Brandes, J. Kirschbaum, W. Wegscheider and M. Bichler and J. P. Kotthaus; "Single-Electron-Phonon Interaction in a Suspended Quantum Dot Phonon Cavity," *Phys. Rev. Lett.*, **92**, 046804 (2004)
- Wu, X. and M. P. Bruchez; "Labeling Cellular Targets with Semiconductor Quantum Dot Conjugates," *Methods Cell Biology*, vol. 75, Cytometry, 4th ed., pp. 171–183, Academic Press, New York, U.S.A. (2004)
- Xu, H., M. Y. Sha, E. Y. Wong, J. Uphoff, Y. Xu, J. A. Treadway, A. Truong, E. O'Brien, S. Asquith, M. Stubbins, N. K. Spurr, E. H. Lai and W. Mahoney; "Multiplexed SNP Genotyping Using the Qbead System: A Quantum Dot-Encoded Microsphere-Based Assay," *Nucleic Acids Res.*, **31**, e43 (2003)
- Zrenner, A., E. Beham, S. Stufler, F. Findeis, M. Bichler and G. Abstreiter; "Coherent Properties of a Two-Level System Based on a Quantum-Dot Photodiode," *Nature*, **418**, 612–614 (2002)

## Water-Soluble Photoluminescent Silicon Quantum Dots\*\*

Jamie H. Warner, Akiyoshi Hoshino, Kenji Yamamoto, and Richard D. Tilley\*

The quantum confinement of excitons in semiconductor quantum dots leads to interesting optical properties that can be exploited in a range of photonic applications including biological fluorescence imaging<sup>[1–6]</sup> and optoelectronic devices.<sup>[7–13]</sup> Quantum dots are becoming popular as replacements for fluorescent dyes in biological fluorescence imaging because of their superior stability against photobleaching. To date, considerable emphasis has been placed on using CdSe quantum dots with a ZnS shell as biological chromophores since they emit light that can be tuned throughout the visible spectrum.<sup>[14]</sup> However, concerns have been raised about the toxicological issue of using cadmium in biological systems.<sup>[15]</sup> In particular, Derfus et al. showed that CdSe quantum dots without a ZnS shell were toxic to liver cells after exposure to UV light.<sup>[15]</sup> The potential biocompatibility of silicon makes photoluminescent silicon quantum dots an ideal candidate for biological fluorescence imaging and should eliminate any potential toxicology problems that might arise from having a CdSe core.<sup>[16, 17]</sup>

Strong quantum confinement in silicon increases the probability of radiative recombination through the direct band gap transitions and reduces phonon-assisted indirect band gap transitions.<sup>[18]</sup> In silicon, this requires the physical dimensions of the quantum dots to be on the order of or less than the bulk exciton Bohr radius of 4 nm.<sup>[19, 20]</sup> Quantum dot sizes of less than 8 nm are easily achieved using wet chemistry techniques.<sup>[19–22]</sup> The remarkably successful advances in the synthesis of the semiconductor groups II/VI and III/V have not been applied to silicon as a consequence of the relatively high temperatures required to degrade the precursor and to produce highly crystalline quantum dots. The greatest success in producing silicon quantum dots with strong quantum confinement to date has been by the solution-phase reduction of silicon salts.<sup>[19, 21, 22]</sup>

The solution-phase synthesis of silicon quantum dots has previously been reported by Kauzlarich and co-workers<sup>[21, 22]</sup> through the use of a variety of reducing agents, by Korgel and co-workers<sup>[19, 23]</sup> through the use of high temperatures and pressures, and by Wilcoxon et al. by using micelles.<sup>[20, 24]</sup> The current problem associated with the simpler room-temperature syntheses<sup>[20–22]</sup> is the large size distribution produced. The large size distribution prevents a simple interpretation of the optical spectra. Post-synthesis treatments for narrowing the size distribution of the silicon quantum dots, such as high-pressure gas chromatography (HPGC), have revealed sharp features in the absorption spectra and narrow photoluminescence spectra attributed to direct band gap transitions.<sup>[20]</sup> We have recently reported the synthesis of 1–2-nm silicon quantum dots that were surface-passivated by 1-heptene. These dots had a narrower size distribution than previously reported and gave a strong blue photoluminescence.<sup>[25]</sup>

For silicon quantum dots to be used in biomedical applications it is essential that they have a substantial photoluminescence quantum yield in the visible region, have a fast radiative recombination rate, and are water soluble and hydrophilic to prevent aggregation and precipitation in a biological environment. The chemical process used to terminate the surfaces of the silicon quantum dots changes the internal electronic structure and thus plays an important role in the resultant emission wavelength and radiative lifetime, and ultimately determines the solubility.<sup>[18]</sup> Silicon quantum dots with an oxide surface passivation typically display a dipole-forbidden yellow-red emission with radiative lifetimes of  $10^{-3}$ – $10^{-6}$  s.<sup>[18, 26]</sup> This slow rate of recombination limits the use of oxide-passivated silicon quantum dots in biological imaging. However, silicon quantum dots with a hydrogen or carbon surface passivation have electric-dipole-allowed direct band gap transitions that lead to blue photoluminescence with fast recombination rates of  $10^8$ – $10^9$  s.<sup>[18, 20]</sup>

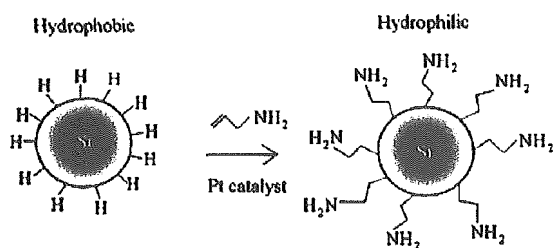
In this study we describe a simple room-temperature synthesis for producing water-soluble silicon quantum dots that exhibit strong blue photoluminescence with a rapid rate of recombination. The use of hydride reducing agents in these experiments produce hydrogen-terminated particle surfaces.<sup>[20, 24, 25]</sup> The Si–H surface bond can then be treated with both a compound containing a C=C bond and a platinum catalyst to produce a variety of surface types through formation of a Si–C surface bond. The surface of the silicon quantum dots are modified with allylamine to form hydrophilic silicon quantum dots (Figure 1). Previous reports of changing the surface-capping molecules of silicon particles have involved treating chloride-terminated particle surfaces with Grignard reagents to produce particles capped with organic molecules<sup>[27]</sup> or utilized a Si–OR bond.<sup>[22]</sup> Silicon quantum dots with a chlorine-terminated surface are restricted to a small range of available Grignard reagents, whilst Si–OR bonds have been shown to greatly affect the electronic charge distribution in the silicon quantum dots and consequently reduce the energy of indirect transitions.<sup>[18, 26]</sup>

Figure 2 shows a high-resolution transmission electron microscope (HRTEM) image of a number of allylamine-capped silicon quantum dots on a carbon-coated copper grid.

[\*] J. H. Warner, R. D. Tilley  
School of Chemical and Physical Sciences  
MacDiarmid Institute of Advanced Materials and Nanotechnology  
Victoria University of Wellington  
P.O. Box 600, Wellington (New Zealand)  
Fax: (+64) 4-463-5237  
E-mail: richard.tilley@vuw.ac.nz

A. Hoshino, K. Yamamoto  
Department of Medical Ecology and Informatics  
Research Institute  
International Medical Center of Japan  
Toyama 1-21-1, Shinjuku, Tokyo 162-8655 (Japan)

[\*\*] J.W. and R.D.T. thank the MacDiarmid Institute of Advanced Materials and Nanotechnology for funding. J.W. and R.D.T. thank H. Rubinsztein-Dunlop for the use of the time-resolved PL spectroscopy system at The University of Queensland.



**Figure 1.** Schematic diagram of the procedure used to change the surface chemistry of the silicon quantum dots from hydrogen to allylamine.

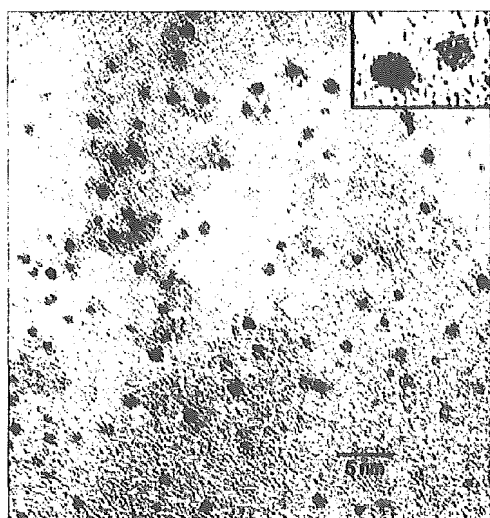


**Figure 2.** High-resolution transmission electron microscopy (HRTEM) image of a large number of allylamine-capped silicon quantum dots. Inset: HRTEM image of two silicon quantum dots showing the crystal lattice planes.

The water-soluble silicon quantum dots were highly crystalline and the atomic lattice planes of two separate silicon quantum dots can be clearly seen in the inset of Figure 2. Fast Fourier transform (FFT) analysis of the crystal structure shown in the inset of Figure 2 could be matched with the (2,1,-1) and (2,-1,1) planes of diamond silicon when viewed down the [011] direction. The low atomic weight of silicon relative to other metallic and semiconductor quantum dots combined with their extremely small dimensions resulted in low contrast in the HRTEM images. Only by removing almost all of the surfactant (TOAB) could such small (1–2 nm) silicon quantum dots be imaged by HRTEM. Figure 2 shows a relatively high contrast HRTEM image of the 1–2-nm silicon quantum dots along with minimal surfactant, thus indicating that a high level of purification had been achieved. The high purity of the silicon quantum dots enables the photoluminescence to be assigned to the quantum dots and not to other by-products of the reaction, such as silicon-based organosilane polymer/oligomers.

The small dimensions of the silicon quantum dots limits the selected-area electron-diffraction and X-ray diffraction measurements, and no conclusive results have as yet been

obtained by using these techniques. The silicon quantum dots were also faceted, which reflects the controlled growth environment.<sup>[19]</sup> A mean size and size distribution of  $1.4 \pm 0.3$  nm of the allylamine-capped silicon quantum dots was obtained by analyzing 648 quantum dots from different regions on the TEM grid. This small size distribution is a significant improvement on previous reports of 1–2-nm silicon quantum dots synthesized in inverse micelles.<sup>[20–22]</sup> Energy-dispersive X-ray spectroscopy (EDS) performed on the quantum dots showed a strong peak associated with silicon and no peaks for platinum. This observation confirmed that the platinum catalyst had successfully been removed during purification.

The bonding of allylamine to the surface of the silicon quantum dots was confirmed by FTIR spectroscopy (Figure 3). Peaks were observed at 1460 and 1260  $\text{cm}^{-1}$  and

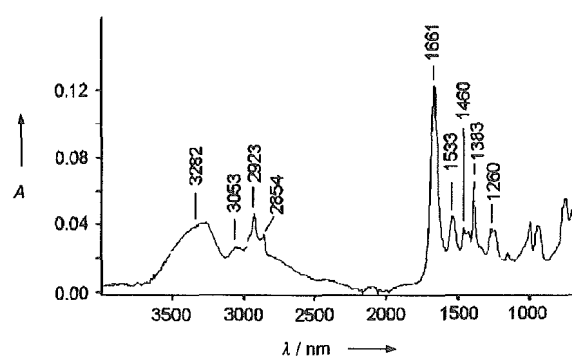


**Figure 3.** FTIR spectrum of allylamine-capped silicon quantum dots.

attributed to the vibrational scissoring and symmetric bending of  $\text{Si-CH}_2$ .<sup>[27]</sup> The absorbance between 2500 and 3500  $\text{cm}^{-1}$  is attributed to symmetric and asymmetric vibrations of the  $\text{C-CH}_2$  and  $\text{C-NH}_3$  molecular components of the allylamine, while the dominant peak at 1661  $\text{cm}^{-1}$  is attributed to the allylamine and clearly indicates its attachment to the silicon quantum dots. The peaks between 1000 and 1100  $\text{cm}^{-1}$  are attributed to the vibrational stretching of  $\text{Si-OR}$ .<sup>[21]</sup> Despite the fact that the silicon quantum dots were heated in atmospheric conditions to remove the solvent for FTIR measurements, the magnitude of the  $\text{Si-OR}$  vibration is very small when compared to the FTIR reports of siloxane-coated silicon quantum dots, which have a total  $\text{Si-OR}$  surface coverage.<sup>[21]</sup> This difference highlights the strength and stability of the  $\text{Si-C}$  bond formed between the silicon quantum dots and the allylamine as well as the minimal number of  $\text{Si-OR}$  surface bonds present.

The absorption spectrum of the allylamine-capped silicon quantum dots in water (Figure 4 a, curve I) displays a feature at 320 nm which is attributed to the  $\Gamma\text{-}\Gamma$  direct band gap transition.<sup>[19,20]</sup> This direct band gap transition has blue-shifted because of the effect of quantum confinement in the quantum dots—from the bulk value of 3.4 to 3.8 eV in these silicon quantum dots—and is in good agreement with other reports.<sup>[19,20]</sup>

The photoluminescence (PL) spectra recorded at 300 and 400 nm (Figures 4 a, curves II and III) show a peak at 480 nm

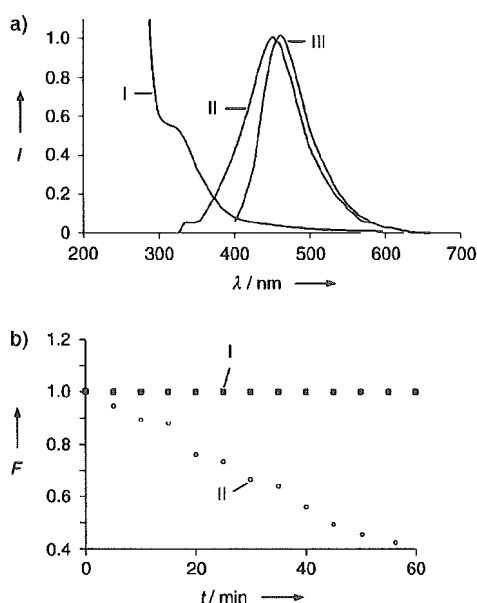


**Figure 4.** a) Curve I: Absorption spectrum of allylamine-capped silicon quantum dots in water; curve II: photoluminescence spectrum of allylamine-capped silicon quantum dots in water with excitation at 300 nm; curve III: photoluminescence spectrum of allylamine-capped silicon quantum dots in water with excitation at 400 nm. b) Integrated photoluminescence as a function of time of allylamine-capped silicon quantum dots in water (curve I) and rhodamine 6G in water (curve II). An excitation wavelength of 400 nm was used in both cases.

with a full-width at half maximum height (FWHM) of 70–80 nm. All the spectra in Figure 4 have been scaled for clarity of presentation.

Photoluminescence quantum yields of the allylamine-capped silicon quantum dots in water were obtained by using the comparative method of Williams et al.<sup>[28]</sup> PL quantum yields of up to 10% were obtained relative to the standard, 9,10-diphenylanthracene, in cyclohexane.<sup>[29]</sup> The optical properties of the colloidal solutions of the allylamine-capped silicon quantum dots were stable for several months. The silicon quantum dots showed better photobleaching stability than the fluorescent dye, rhodamine 6G in water, on excitation with UV light (Figure 4b). The silicon quantum dots showed no signs of any measurable photobleaching (Figure 4b, curve I) under the same illumination conditions during which the photoluminescence from rhodamine 6G dropped by 60% (Figure 4b, curve II).

The origin of the photoluminescence observed in Figure 4 is complicated by the combination of both indirect and direct band gap transitions present in silicon quantum dots and is actively debated.<sup>[19]</sup> However, there is strong theoretical evidence suggesting that 1–2-nm silicon quantum dots with a hydrogen or carbon surface termination have direct band gap optical transitions that lead to photoluminescence in the UV/blue region of the electronic spectrum.<sup>[18]</sup> The emission observed in Figure 4a is consistent with the theoretical predictions of direct band gap recombination in silicon quantum dots with carbon surface termination rather than from trap states or surface states, or of silicon quantum dots

with oxygen surface termination. Emission from a Si–OR-terminated silicon quantum dot is typified by an emission centered at 600 nm.<sup>[20,30]</sup>

Further insights into the nature of the photoluminescence can be obtained by analyzing the time-resolved photoluminescence spectra from the allylamine-capped silicon quantum dots in water. Figure 5 shows the time-resolved photolumi-

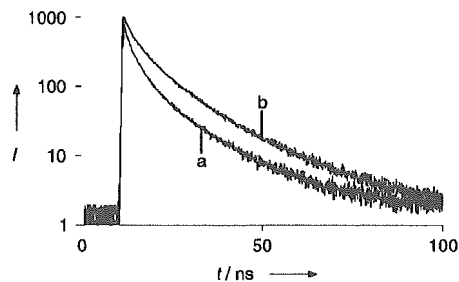


**Figure 5.** Time-resolved photoluminescence decays of allylamine-capped silicon quantum dots in water measured at emission wavelengths a) 420 nm and b) 500 nm. An excitation wavelength of 380 nm was used.

nescence decays from an aqueous solution of allylamine-capped silicon quantum dots at two different emission wavelengths. The PL decay measured at 420 nm (Figure 5, curve a) is noticeably shorter than the PL decay measured at 500 nm in curve b. Both PL decays required a three exponential fit with an overall average decay of 4 ns.

Indirect band gap materials, such as silicon, generally have slow recombination with PL lifetimes on the order of tens of microseconds to milliseconds, whereas direct band gap materials, such as GaAs and CdSe, have fast recombination with PL lifetimes on the order of 1–10 ns.<sup>[31]</sup> The PL lifetime measurements obtained here are in good agreement with the experimental findings of the research groups of Korgel<sup>[23]</sup> and Wilcoxon<sup>[20]</sup> as well as the theoretical predictions of Zhou et al.<sup>[18]</sup> The rapid rates of recombination measured here provide strong evidence that the observed emission results from dipole-allowed recombination across the direct band gap transition in silicon quantum dots with a carbon surface termination.

The suitability of allylamine-capped silicon quantum dots as a chromophore for biological imaging is demonstrated in Figure 6, for which an excitation wavelength of 365 nm was used and the emission at 480 nm was monitored. The control image (Figure 6a) shows minimal fluorescence from the HeLa cells relative to the HeLa cells with the incorporated silicon quantum dots (Figure 6b). Thus, the fluorescence observed in the HeLa cells in Figure 6b arises from the emission from silicon quantum dots and not autofluorescence from the cells. The inset in the top left corner of Figure 6b shows the bright blue fluorescence from a vial of allylamine-capped silicon quantum dots in water when excited with UV light. The bright blue fluorescence from the silicon quantum dots is distributed uniformly inside the cytosol of the HeLa cells and this shows the possibility of using these hydrophilic silicon quantum dots as chromophores in biological fluores-

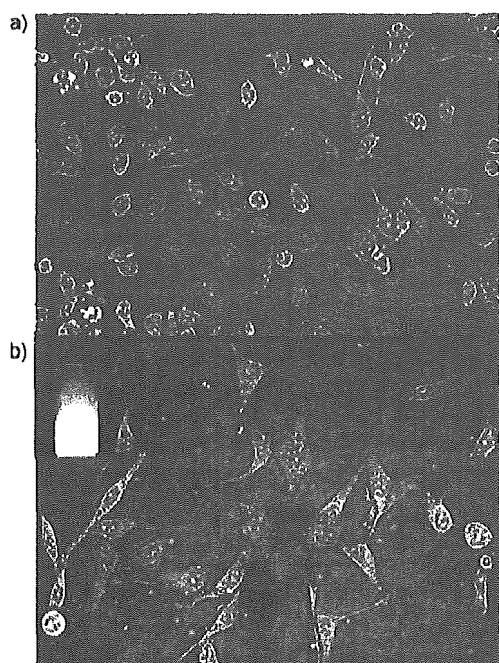


**Figure 6.** Overlay of the transmission and fluorescence microscope images of a) HeLa cells in the absence of any quantum dots and b) HeLa cells with silicon quantum dots incorporated inside the cytosol. Inset: fluorescence from a vial of allylamine-capped silicon quantum dots in water when excited with a UV lamp.

cence imaging. This result has major implications towards using colloidal silicon quantum dots effectively in biological fluorescence imaging.

In summary, silicon quantum dots with a narrow size distribution were synthesized using reverse micelles and powerful hydride reducing agents at room temperature and pressure. The surface of the silicon quantum dots was made hydrophilic by modification with allylamine. The silicon quantum dots dispersed in an aqueous environment displayed strong photoluminescence in the blue region of the visible spectrum, with a 10% quantum yield for the photoluminescence. The optical properties of the silicon quantum dots displayed features in both the absorption and emission spectra attributed to the direct band gap transitions in silicon quantum dots with a carbon surface termination. Time-resolved photoluminescence spectroscopy revealed a rapid recombination normally associated with direct band gap materials. The ease of synthesis and optical properties make the silicon quantum dots reported here excellent candidates for biomedical applications, as demonstrated by the imaging of allylamine-capped silicon quantum dots in HeLa cells.

### Experimental Section

**Synthesis of allylamine-capped silicon quantum dots:** Silicon quantum dots were synthesized in reverse micelles by the solution-phase reduction of  $\text{SiCl}_4$  with  $1\text{ M LiAlH}_4$  in THF (Aldrich). The surfactant and solvent combination used to form the micelles were tetraoctylammonium bromide (TOAB, Merck) in toluene. Surface modification of the silicon quantum dots was achieved by treating the surface

of the particles with allylamine (Aldrich). All experiments were carried out in an argon atmosphere in a glove box to prevent oxidation of the silicon. Oxygen levels were below 10 ppm at all times.

In a typical experiment,  $\text{SiCl}_4$  (92  $\mu\text{L}$ , 0.0008 mol) was dissolved in TOAB (1.5 g) and anhydrous toluene (100 mL) by using a homogenizer. Silicon quantum dots were then formed by adding a twofold excess of reducing agent. The mixture was left to react for 3 h and then anhydrous methanol (20 mL) was slowly added to quench any excess reducing agent. At this point it is expected that the surface of the particles were terminated with hydrogen.<sup>[20,25]</sup> Hydrophilic particles were formed by modifying the surface silicon–hydrogen bonds by reaction with 0.05 M  $\text{H}_2\text{PtCl}_6$  (40  $\mu\text{L}$ ) in isopropanol as the catalyst and allylamine (2 mL). After modification of the surface, the sample was removed from the glove box and purified by removing the surfactant.<sup>[32]</sup> The solvent was then removed using a rotary evaporator to produce a white powder consisting of mainly TOAB and silicon quantum dots. Distilled water (50 mL) was then added to the flask and resulted in the hydrophilic silicon quantum dots dissolving, but not the TOAB. The TOAB was then removed by successive filtration through a 0.22- $\mu\text{m}$  membrane filter.

**Incorporation of silicon quantum dots into HeLa cells:** The HeLa cells were cultured in DMEM/F12 supplemented with 10% heat-inactivated fetal bovine serum at 37°C. The cells were plated at a volume of  $1 \times 10^6$  cells/well on a 6-well culture plate (Iwaki technoglass, Japan) and were stimulated with a solution of 0.2 nM Si quantum dots. After incubation of the mixtures for 12 h, the cells were washed with a phosphate-buffered saline (PBS) twice to remove the nonspecific binding quantum dots. The cells were then fixed with 1% paraformaldehyde in PBS for 5 min.<sup>[33]</sup> Fluorescence images of the HeLa cells were acquired with a digital camera D1X (Nikon) on a fluorescent microscope IX-81 (Olympus) using a mirror unit to adjust the excitation wavelength to 365 nm and an oil immersion objective lens. The blue fluorescent light was detected in the cytosol of each cell.

Received: April 11, 2005

Published online: ■■■ ■■■, ■■■■■■

**Keywords:** imaging agents · luminescence · nanostructures · quantum dots · silicon

- [1] W. C. Chan, S. Nie, *Science* **1998**, *281*, 2016.
- [2] M. Bruchez, M. Moronne, P. Gin, S. Weiss, A. P. Alivisatos, *Science* **1998**, *281*, 2013.
- [3] M. Green, *Angew. Chem.* **2004**, *116*, 4221; *Angew. Chem. Int. Ed.* **2004**, *43*, 4129.
- [4] A. Wu, H. Liu, J. Liu, K. N. Haley, J. A. Tradway, J. P. Larson, N. Ge, F. Peale, M. P. Bruchez, *Nat. Biotechnol.* **2003**, *21*, 41.
- [5] B. Dubertret, P. Skourides, D. J. Norris, V. Noireaux, A. H. Brivanlou, A. Libchaber, *Science* **2002**, *298*, 1759.
- [6] D. R. Larson, W. R. Zipfel, R. M. Williams, S. W. Clark, M. P. Bruchez, F. W. Wise, W. W. Webb, *Science* **2003**, *300*, 1434.
- [7] L. Bakueva, G. Konstantatos, L. Levina, S. Musikhin, E. H. Sargent, *Appl. Phys. Lett.* **2004**, *84*, 3459.
- [8] S. A. McDonald, P. W. Cyr, L. Levina, E. H. Sargent, *Appl. Phys. Lett.* **2004**, *85*, 2089.
- [9] S. Coe, W. Woo, M. Bawendi, V. Bulovic, *Nature* **2002**, *420*, 800.
- [10] T. Tsutsui, *Nature* **2002**, *420*, 752.
- [11] W. U. Huynh, J. J. Dittmer, A. P. Alivisatos, *Science* **2002**, *295*, 2425.
- [12] R. A. M. Hikmet, D. V. Talapin, H. Weller, *J. Appl. Phys.* **2003**, *93*, 3509.
- [13] B. Sun, E. Marx, N. C. Greenham, *Nano Lett.* **2003**, *3*, 961.
- [14] C. B. Murray, D. J. Norris, M. G. Bawendi, *J. Am. Chem. Soc.* **1993**, *115*, 8706.

## Communications

- [15] A. M. Derfus, W. C. W. Chan, S. N. Bhatia, *Nano Lett.* **2004**, *4*, 11.
- [16] D. K. Nagesha, M. A. Whitehead, J. L. Coffey, *Adv. Mater.* **2005**, *17*, 921.
- [17] L. T. Canham, C. L. Reeves, J. P. Newey, M. R. Houlton, T. I. Cox, J. M. Buriak, M. P. Stewart, *Adv. Mater.* **1999**, *11*, 1505.
- [18] Z. Zhou, L. Brus, R. Friesner, *Nano Lett.* **2003**, *3*, 163.
- [19] J. D. Holmes, K. J. Ziegler, C. Doty, L. E. Pell, K. P. Johnson, B. A. Korgel, *J. Am. Chem. Soc.* **2001**, *123*, 3748.
- [20] J. P. Wilcoxon, P. P. Provencio, G. A. Samara, *Phys. Rev. B* **1999**, *60*, 2704.
- [21] R. K. Baldwin, K. A. Pettigrew, E. Ratai, M. P. Augustine, S. M. Kauzlarich, *Chem. Commun.* **2002**, 1822.
- [22] J. Zou, R. K. Baldwin, K. A. Pettigrew, S. M. Kauzlarich, *Nano Lett.* **2004**, *4*, 1181.
- [23] D. S. English, L. E. Pell, Z. Yu, P. F. Barbara, B. A. Korgel, *Nano Lett.* **2002**, *2*, 681.
- [24] J. P. Wilcoxon, G. A. Samara, *Appl. Phys. Lett.* **1999**, *74*, 3164.
- [25] R. D. Tilley, J. H. Warner, K. Yamamoto, I. Matsui, H. Fujimori, *Chem. Commun.* **2005**, *14*, 1836.
- [26] A. Puzder, A. J. Williamson, J. C. Grossman, G. Galli, *J. Am. Chem. Soc.* **2003**, *125*, 2786.
- [27] C. Yang, R. A. Bley, S. M. Kauzlarich, H. W. H. Lee, G. R. Delgado, *J. Am. Chem. Soc.* **1999**, *121*, 5191.
- [28] A. T. R. Williams, S. A. Winfield, J. N. Miller, *Analyst* **1983**, *108*, 1067.
- [29] S. Hamai, F. Hirayama, *J. Phys. Chem.* **1983**, *87*, 83.
- [30] Y. Kanemitsu, T. Futagi, T. Matsumoto, H. Mimura, *Phys. Rev. B* **1994**, *49*, 14732.
- [31] J. H. Warner, E. Thomsen, A. R. Watt, N. R. Heckenberg, H. Rubinsztein-Dunlop, *Nanotechnology* **2005**, *16*, 175.
- [32] R. D. Tilley, S. Saito, *Langmuir* **2003**, *19*, 5115.
- [33] A. Hoshino, K. Fujioka, T. Oku, M. Suga, Y. F. Sasaki, T. Ohta, M. Yasuhara, K. Suzuki, K. Yamamoto, *Nano Lett.* **2004**, *4*, 2163.



Editor-Communicated Paper

# Simultaneous Multicolor Detection System of the Single-Molecular Microbial Antigen with Total Internal Reflection Fluorescence Microscopy

Akiyoshi Hoshino<sup>1,2</sup>, Kouki Fujioka<sup>1</sup>, Noriyoshi Manabe<sup>1</sup>, Shun-ichi Yamaya<sup>1</sup>, Yoji Goto<sup>3</sup>, Masato Yasuhara<sup>2</sup>, and Kenji Yamamoto<sup>\*,1,2</sup>

<sup>1</sup>Department of Medical Ecology and Informatics, Research Institute, International Medical Center of Japan, Shinjuku-ku, Tokyo 162–8655, Japan, <sup>2</sup>Department of Pharmacokinetics and Pharmacodynamics, Hospital Pharmacy, Tokyo Medical and Dental University Graduate School, Bunkyo-ku, Tokyo 113–8519, Japan, and <sup>3</sup>Research Center for Biologicals, The Kitasato Institute, Kitamoto, Saitama 364–0026, Japan

Communicated by Dr. Hidechika Okada: Received February 25, 2005. Accepted March 1, 2005

**Abstract:** Immunological diagnostic methods have been widely performed and showed high performance in molecular and cellular biology, molecular imaging, and medical diagnostics. We have developed novel methods for the fluorescent labeling of several antibodies coupled with fluorescent nanocrystal QDs. In this study we demonstrated that two bacterial toxins, diphtheria toxin and tetanus toxin, were detected simultaneously in the same view field of a cover slip by using directly QD-conjugated antibodies. We have succeeded in detecting bacterial toxins by counting luminescent spots on the evanescent field with using primary antibody conjugated to QDs. In addition, each bacterial toxin in the mixture can be separately detected by single excitation laser with emission band pass filters, and simultaneously *in situ* pathogen quantification was performed by calculating the luminescent density on the surface of the cover slip. Our results demonstrate that total internal reflection fluorescence microscopy (TIRFM) enables us to distinguish each antigen from mixed samples and can simultaneously quantitate multiple antigens by QD-conjugated antibodies. Bioconjugated QDs could have great potentialities for in practical biomedical applications to develop various high-sensitivity detection systems.

**Key words:** Simultaneous multicolor detection, Single-molecular microbial antigen, TIRFM, Quantum dot

The high sensitivity detection system, which detects the smaller amounts of chemicals and biomolecules, is a prospective technology and can be applied not only for medical application but for the preparations and responses in case of emergency in various fields; environmental technology, water poisoning, safety of food and drug supply, and public health security such as preparation against bioterrorism. However, a lot of processes are required to detect these smaller amounts of harmful substances. Hence, there is a problem to require much time in detection of biomolecules.

The immunological diagnostic methods were widely performed in the medical field. In these cases, almost

all of the samples are provided as blood, tissue, exudation fluid, or excrement, and the antigen-antibody reaction was commonly performed as the detection method in addition to the colorimetric methods. In this article we developed a high sensitive and quick antigen detecting system using the fluorescence nanocrystal quantum dots (QDs) about a substance detrimental to the biomolecules, such as a bacterial toxin that caused food poisoning or bioterrorism. In order to detect bacterial toxins sensitively and quickly, we adapted the fluorescence-ELISA using QDs to the origin of evanescent microscopy. In this system, the fluorescence of the QD-conjugated antibody, which detects bacterial toxins, is placed on the evanescent field, resulted in detecting bacterial toxins countable by single molecules. Imaging

\*Address correspondence to Dr. Kenji Yamamoto, Department of Medical Ecology and Informatics, Research Institute, International Medical Center of Japan, Toyama 1–21–1, Shinjuku-ku, Tokyo 162–8655, Japan. Fax: +81–3–3202–7364. E-mail: backen@ri.imcj.go.jp

Abbreviations: QD, quantum dot; TIRFM, total internal reflection fluorescent microscopy.

of single fluorescent molecules has been achieved using an objective-type total internal reflection fluorescence microscopy (TIRFM). TIRFM selectively illuminates the aqueous phase immediately adjacent to a glass interface with an exponentially decaying excitation called evanescent waves (1, 23, 24). In TIRFM, also called evanescent wave microscopy, the excitation light typically penetrates <150 nm above the reflecting surface and is ideal for studying the surface of the cellular processes such as cell adhesion.

Nanocrystal quantum dots (QDs) are ultrafine fluorescent-emitting particles that consist of CdSe/ZnS-core/shell semiconductor nanoparticles. QDs have the potential to be applied to bioimaging due to their higher and far longer fluorescence. QDs were widely used in biotechnology and medical applications (3, 4, 7–9, 17–22, 27, 28). Several applications have demonstrated that QDs were adapted for immunoassay and diagnostics (2, 9, 10, 16, 25). QDs have several advantages over organic fluorophores. QDs show high luminance, resistance to photobleaching, a range of exciting wavelength from ultra violet to red that depends on the size of the particles, and cover a range of fluorescent wavelengths from blue to red that can be excited using a mercury arc lamp. At present, many organic fluorophores were used for TIRFM imaging, but experiments using organic dyes are unsuitable for extended periods of bioimaging observations because organic fluorophores tend to quench rapidly (5). In contrast, QDs are stabilized over a far longer exposure-time to light and can emit a fluorescence of high luminosity under almost the equivalent condition as the conventional organic fluorescence probes (15). In this study, we performed the detection of diphtheria toxin and tetanus toxoid by different color-emitting QD-conjugated antibodies, and visualized each toxin within the same view field.

## Materials and Methods

**Antigens, antibodies, and reagents.** Four target proteins; casein from bovine milk, equine cytochrome-*c*, lysozyme, and ovalbumin from chicken egg, were purchased from Sigma-Aldrich (St. Louis, Mo., U.S.A.). Antibodies for lysozyme and ovalbumin were purchased from Rockland, Inc. (Gilbertsville, Penn., U.S.A.), ones for cytochrome-*c* was from Nordic Immunological Laboratories (Tilburg, Netherlands). Diphtheria toxin and anti-diphtheria toxin antibody (human) were provided by Toyo Public Health College (Tokyo). Anti-tetanus toxin antibody was purchased from Biogenesis (Poole, England, U.K.). Tetanus toxin, human HBs antigen, and sheep antiserum for HBs anti-

gen were provided by Kitasato Institute (Tokyo). Anti-HBs antibody was purified by Hi-Trap protein G column (Amersham Pharmacia, Uppsala, Sweden). All the antibodies used in this study were directly labeled with QDs as described below.

**Preparation of antibody-conjugated QDs.** ZnS-capped CdSe core-shell nanocrystal QDs (fluorescence wavelength: approximately 642 nm emitted red, and approximately 518 nm emitted green), were enfolded into the micelle of *n*-trioctylphosphine oxide (TOPO), according to general methods (6, 12). Then the hydrophilic QDs (carboxyl-QDs) were produced by thiol exchange reaction (13). The antibodies described above were conjugated to QDs by the two-step reaction as described previously (14). QD solution was primarily mixed with cysteine solution in coexistent with 1-ethyl-3-(3-dimethylaminopropyl)-carbodiimide cross-linking reagents (EDC, Pierce Biotechnology, Rockford, Ill., U.S.A.) and mixed under the chilled condition, and secondarily coupled with target antibodies by attaching succinimidyl 4-(*N*-maleimidomethyl)cyclohexane-1-carboxylate (SMCC, Pierce Biotech) under sonicated condition. The products were purified using Superdex200® gel filtration column (Amersham Biosciences, Piscataway, Ill., U.S.A.). Finally, purified QD-peptide conjugates were concentrated by Ultrafree®-biomax centrifugal filter devices (Millipore, Bedford, Mass., U.S.A.). To analyze the protein content of QD-conjugated peptides, conjugated QDs were plated to 96-well microplate and RC-DC Protein Assay reagent (Bio-Rad, Hercules, Calif., U.S.A.) was added. After incubation for 1 hr, 650 nm absorbance was measured by microplate reader (Bio-Rad). Hydrophilic QD was used as negative control.

**Fluorescent immunoassays.** 0.12 mm-thickness coverslips (Matsunami Glass Industries, Japan) were pre-coated with poly-L-lysine (Peptide Institute Co., Ltd., Osaka, Japan), to avoid the non-specific binding of QDs on the glass. Then target peptides were dissolved in bicarbonate buffer (pH 8.2) and plated on the coverslip at an adequate concentration. After incubation, blocking reaction was performed with 0.2% gelatin in carbonate buffer at 37 C for 30 min. Next, QD-labeled antibodies were added to the plate and incubated at 37 C for 30 min. After washed with PBS 5 times, fluorescence was detected by TIRFM. Quantitation of antigen absorbed on the coverslip was detected by performing ELISA on the glass. Briefly, the coverslip with target peptide was treated with unlabeled primary antibody for 30 min (the same antibody used for QD-conjugation) and secondary reacted with HRP-conjugated secondary antibody for 30 min again (Goat anti-human or rabbit IgGs from Zymed Laboratories, South San Francisco,

Calif., U.S.A.). Then, TMB substrate (KPL Corp., Gaithersburg, Md., U.S.A.) was added to the coverslip. After stopping reaction, 100  $\mu$ l of colored solution was transferred to the 96-well multiplate. Four-hundred and fifty nanometer absorbance (reference; 650 nm) was measured by microplate reader (Bio-Rad). Fluorescence emission on the multiwell plate was measured by fluorescent microplate reader (Fluoroskan Ascent, Thermo Electron Corp., Waltham, Mass., U.S.A.). ELISA on the MaxiSorp<sup>®</sup> 96-well microplate (Nalge Nunc, Naperville, Ill., U.S.A.) was used as standard curve.

**Multi-channel total internal reflection fluorescence microscopy imaging.** Objective-based multi-channel TIRFM was obtained by directing an argon ion 488 nm laser through dichroic mirrors (DM505) and emission filters on an Olympus IX-70 microscope. The laser beam was on the coverslip at 58.4–64.2 degree to the optical axis giving a decay constant of the evanescent field of 48–62 nm. The beam was focused on the periphery of the back focal plane of a 100 $\times$  objective with NA of 1.65 with high refractive index immersion oil (Olympus Corp., Tokyo). The filter cube contained a 488/10 laser clean-up filter in the excitation position, and emission signals were separated using two kinds of optical splitters; Ch1 was with 510–550 bandpass, and Ch2 was with >610 longpass emission filters; the red (Ch2) and green (Ch1) images were simultaneously imaged side by side on a CCD camera. Images were acquired, and the raw stacks were split into single channels using MetaMorph<sup>®</sup> software (Universal Imaging Corp., Marlow, Buckinghamshire, U.K.).

## Results and Discussion

Fluorescent QDs are suitable for multiplexed analyzing tool by using those properties that emits luminescence that depends on their particle size. Multiplexed fluoroimmunoassays using QD has already reported (10, 11). In this study we try to detect antigen-antibody reaction at single molecular level and to achieve the high-sensitive *in situ* antigen quantitation using by an evanescent microscopy. To confirm the assay performance, we first examined the simulation for the detection of each antigen by using ovalbumin, lysozyme, cytochrome-*c*, and antibodies for those antigens. First, ovalbumin was dissolved in bicarbonate buffer contained 1  $\mu$ g/ml casein, and 100  $\mu$ l of solution plated on the cover slip at 1, 0.1, and 0.01  $\mu$ g/ml. Absorbed ovalbumin molecules on the evanescent field were detected by QD-conjugated anti-ovalbumin antibody (Fig. 1a). In TIRFM imaging, every antigen was visible as a fluorescent spot. The fluorescent intensity on TIRFM was measured by counting luminescent spots of the 5

$\mu$ m $\times$ 5  $\mu$ m view field on TIRFM images (Fig. 1b). By using QD-labeled secondary antibody, non-linear fluorescence was observed by microplate reader. On the other hand, linear response still remained on the signal of TIRFM images. Thus, antigen detection using TIRFM has advantages with the exclusion of non-specific signal out of evanescent view fields.

Next, we assessed detection of specific antigen from the mixture of several antigens. The mixture solution of casein, cytochrome-*c*, and ovalbumin was plated on the coverslip. Next ovalbumin was detected by QD-conjugated anti-ovalbumin antibodies (Fig. 2a, left). Fluorescent spots emitted from albumin-antibodies were observed at dose dependent manner. In contrast, luminescent spots from cytochrome-antibodies were not affected by the dose of ovalbumin but by cytochrome (Fig. 2a, right). The same pattern was also detected by cytochrome (Fig. 2b) and casein (data not shown). Then we compare the antigen detection by colorimetric method with HRP-conjugated antibody and by QD-conjugated antibody on TIRFM. A conventional ELISA was performed on the glass-based plate under the same condition performed in Fig. 2, and 450 nm absorbance of colored TMB peroxidase reagents was measured by microplate reader (Fig. 3, filled symbols). These results indicated that the specific antigen could be also detected separately on the evanescent view fields at high performance as well as ELISA.

Then we tried simultaneous detection of two antigens on the same plate by green- and red-emitted QD conjugated antibodies. The mixture of ovalbumin and cytochrome-*c* was plated on the cover slip at the indicated concentration. Ovalbumin and cytochrome-*c* were simultaneously detected by QD640 (emitted red)-labeled anti-ovalbumin or QD520 (emitted green) labeled anti-cytochrome-*c* antibodies. Without using any filters, luminescences from QD520 and QD640 were not distinguished from each other and observed as yellow (merged) images in the view field. In contrast, TIRFM images can detect both signals from QD520 and QD640 simultaneously as luminescent spots (Fig. 4). In addition, emission signals of the green and the red were simultaneously detected by two kinds of optical splitters. Then ovalbumin and cytochrome-*c* were simultaneously detected by the mixture of anti-ovalbumin (QD640) and anti-cytochrome-*c* (QD520) antibodies at dose-dependent manner. Luminescence was divided to red and green channels as described in Fig. 4. These results suggested that these two antigens can be simultaneously detected as green and red luminescent spots and be quantitated by counting luminescence spots by using TIRFM imaging.

Next, we examined whether microbial antigen also

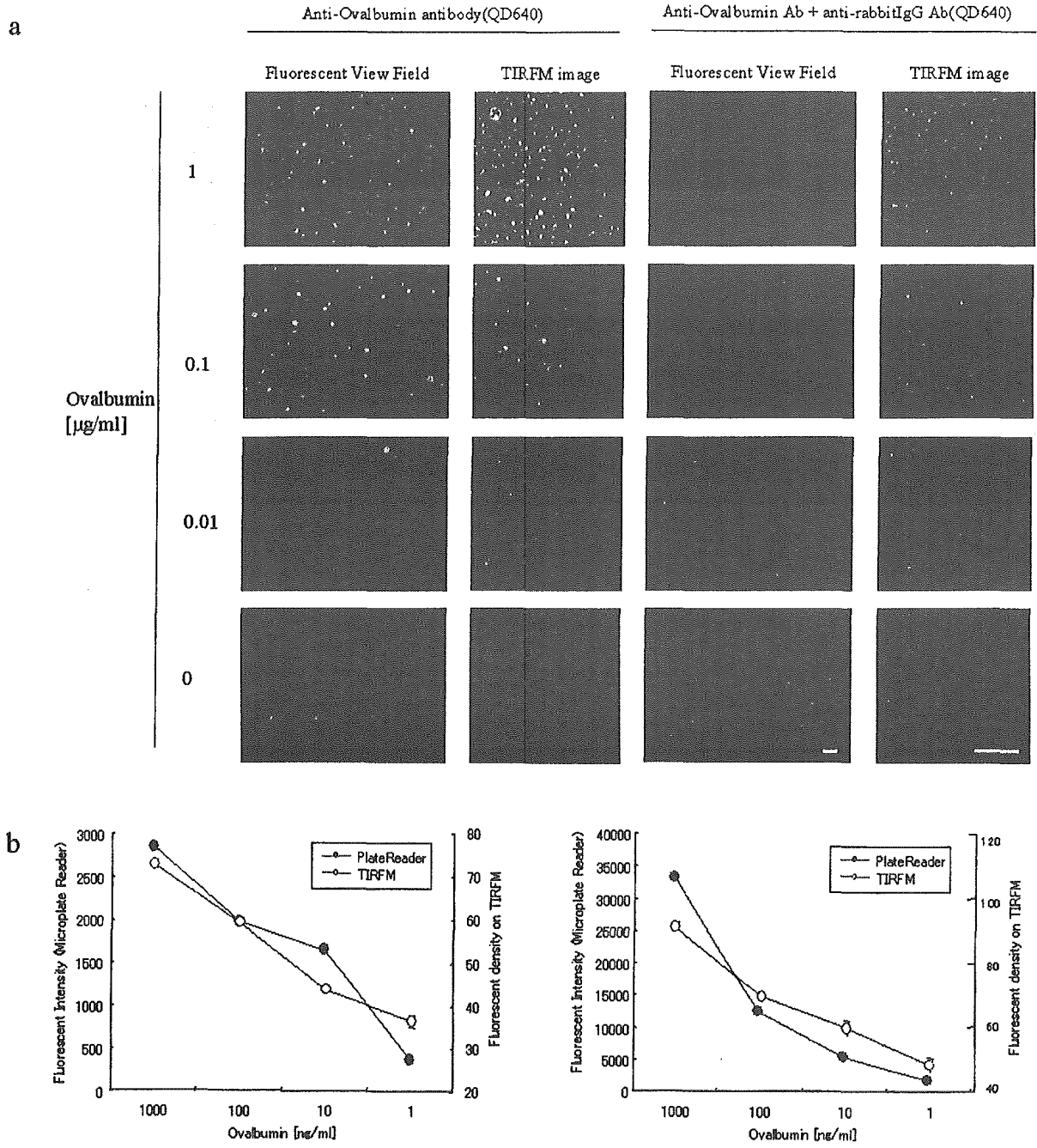


Fig. 1. Antigen detection by QD-conjugated antibody on the evanescent field. (a) TIRFM and fluorescent imaging of antigen. Ovalbumin solution was plated on the cover slip at indicated concentration. Absorbed ovalbumin molecules on the evanescent field were detected by QD-conjugated anti-ovalbumin antibody. The images represent one out of three performed. Bars indicate 10 μm. (b) The fluorescence intensity measured by fluorescent microplate reader is given on the left scale of y-axis and the fluorescent counts on TIRFM are on the right scale of y-axis, respectively. Fluorescence density was performed by counting luminescent spots of the 5 μm×5 μm view field on TIRFM images. The data are presented as the mean ± standard deviation (n=3). Open circles indicate TIRFM counts, and closed circles are fluorescent intensity, respectively.

can be detected by TIRFM. At first, human hepatitis virus antigen (HBs) was plated on the cover slip and detected by QD-conjugated anti-HBs antibody (Fig. 6a). Viral antigen was also detected by TIRFM imaging. Detection sensitivity of HBs by ELISA was shown in Fig. 6b. The sensitivity of ELISA method shows 10

times higher than that of TIRFM imaging. This is caused by the non-specific luminescent spots at background level.

Then we assessed the simultaneous detection of two bacterial toxins by TIRFM. We tried to image the antigen-antibody reaction of diphtheria toxin and tetanus

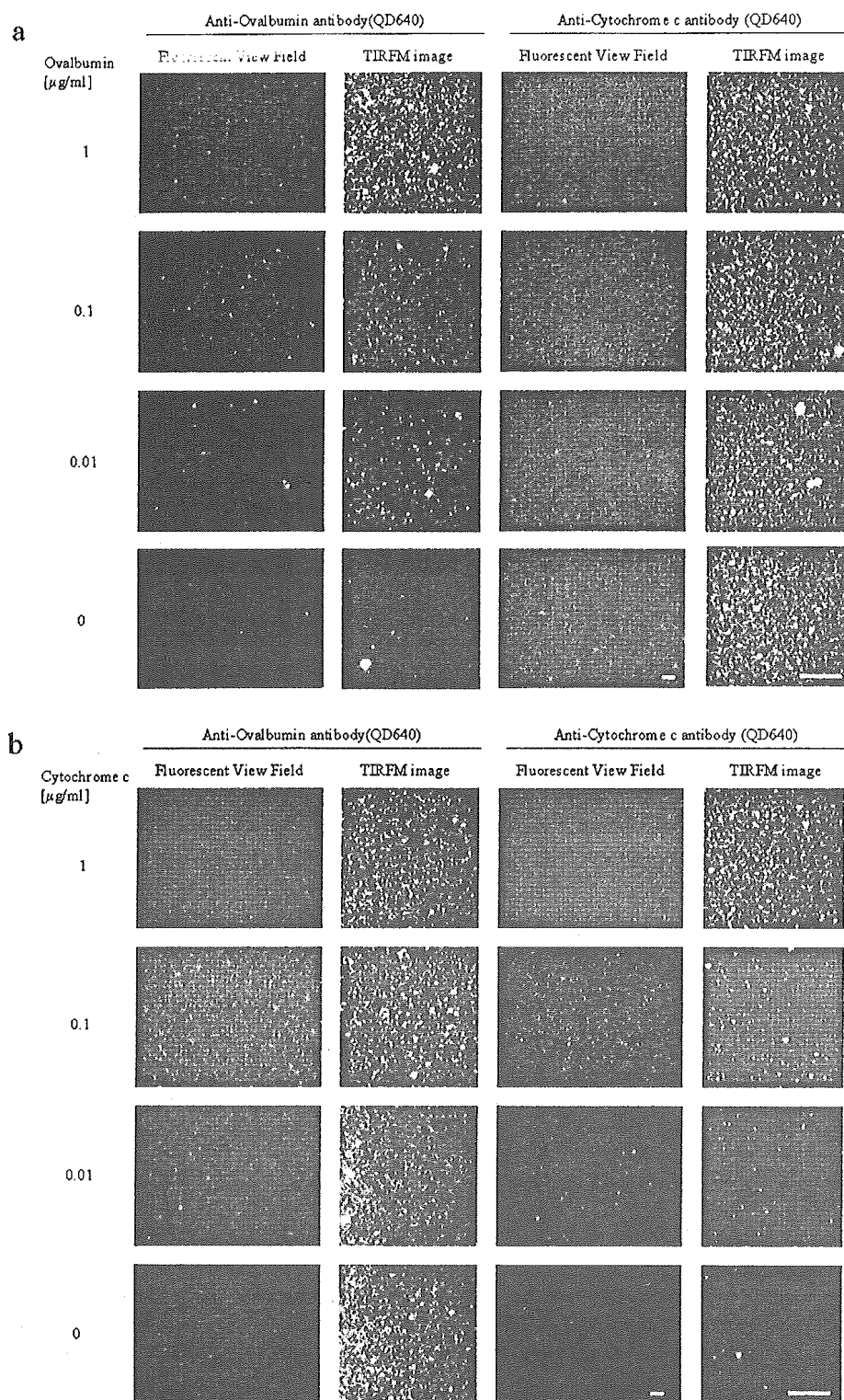


Fig. 2. Two antigens on the evanescent field were detected by QD-conjugated antibody. The mixture of ovalbumin and cytochrome-c was plated on the cover slip at indicated concentration. Each antigen was separately detected by QD-conjugated anti-ovalbumin (a) or anti-cytochrome-c (b) antibodies, as shown in Fig. 1. Shown are data of a representative experiment ( $n=3$ ). Bars indicate 10  $\mu\text{m}$ .

toxin. Mixture of two bacterial toxins were plated on the cover slip at indicated concentrations, and detected by anti-diphtheria toxin (QD520) and anti-tetanus toxin

(QD640) antibodies (Fig. 7a). At the same time, detection sensitivity of diphtheria and tetanus toxins by ELISA was also performed on the glass-base dishes



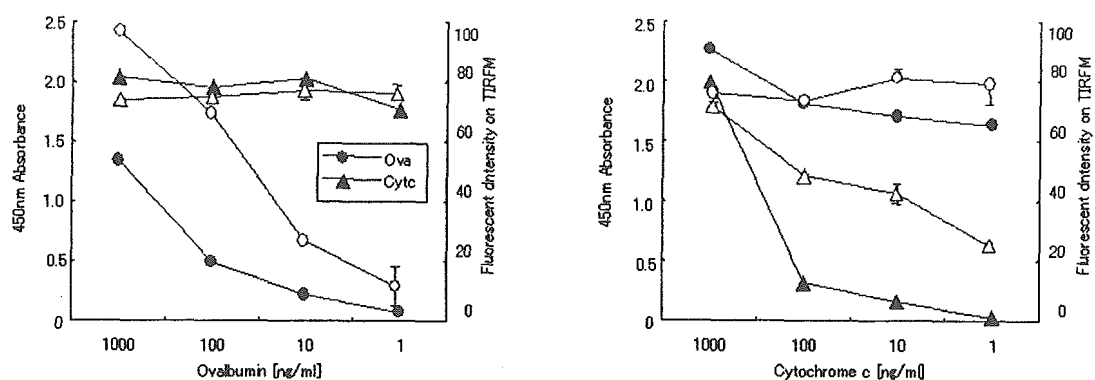


Fig. 3. Comparison of antigen detection by colorimetric method with HRP-conjugated antibody and by QD-conjugated antibody on TIRFM. ELISA of two antigens on the glass-based plate was performed. Absorbance of peroxidase reagents is given on the left scale of y-axis. Values are the means  $\pm$  standard deviation of duplicate experiments. Results were reproduced in three separate experiments. As described in Fig. 1b, the fluorescent counts on TIRFM are on the right scale, respectively. Filled symbols indicated the results of ELISA. Circles and triangles mean ovalbumin and cytochrome-c, respectively.

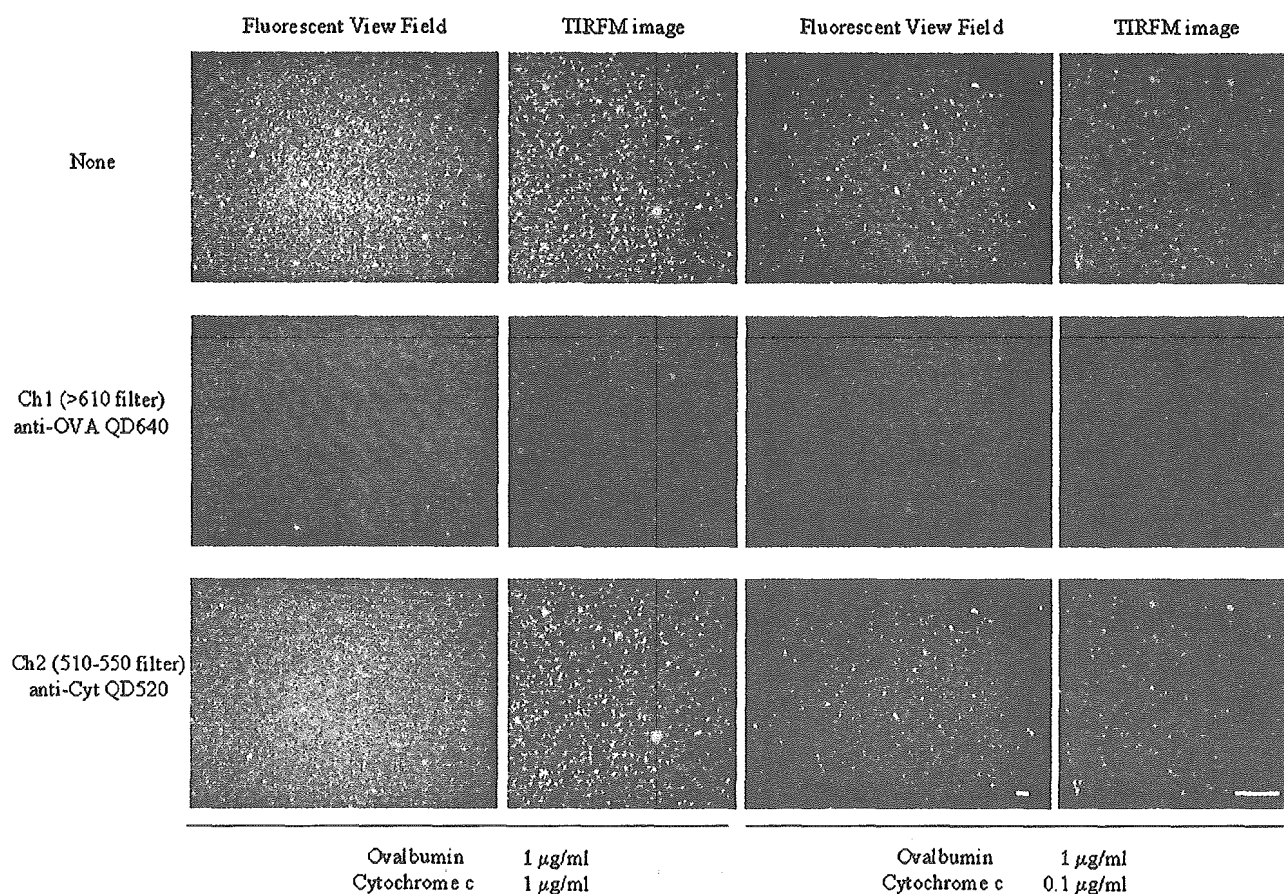


Fig. 4. Two antigens on the same plate were simultaneously detected by green- and red-emitted QD conjugated antibodies. The mixture of ovalbumin and cytochrome-c was plated on the cover slip at indicated concentration. Ovalbumin and cytochrome-c were simultaneously detected by QD640 (emitted red)-labeled anti-ovalbumin or QD520 (emitted green) labeled anti-cytochrome-c antibodies. Luminescence was divided to indicated channels according to the emission wavelengths of QDs. Bars indicate 10  $\mu$ m. None: images without using emission filters.

(Fig. 7b). Anti-diphtheria toxin (human) or anti-tetanus toxin (rabbit) was added, and toxins were detected by human or rabbit HRP-conjugated secondary antibodies. These results suggested that TIRFM method does not

excel the conventional detection system in the sensitivity or certainty. But two bacterial antigens can also be simultaneously detected and quantitated by counting luminescence spots, implying that TIRFM system was

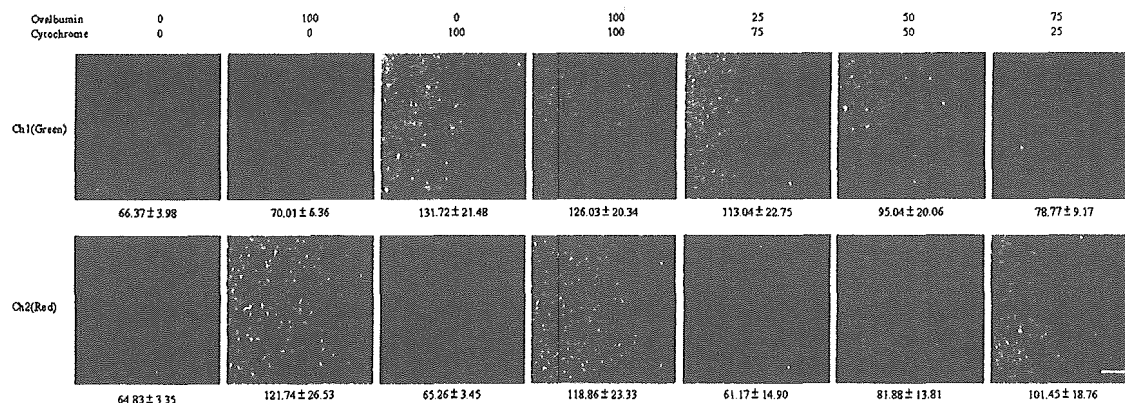


Fig. 5. Two antigens on the same plate were simultaneously detected by green- and red-emitted QD conjugated antibodies. Ovalbumin and cytochrome-*c* were simultaneously detected by the mixture of anti-ovalbumin (QD640) and anti-cytochrome-*c* (QD520) antibodies. Luminescence was divided to red and green channels as described in Fig. 4. Bars indicate 10  $\mu\text{m}$ .

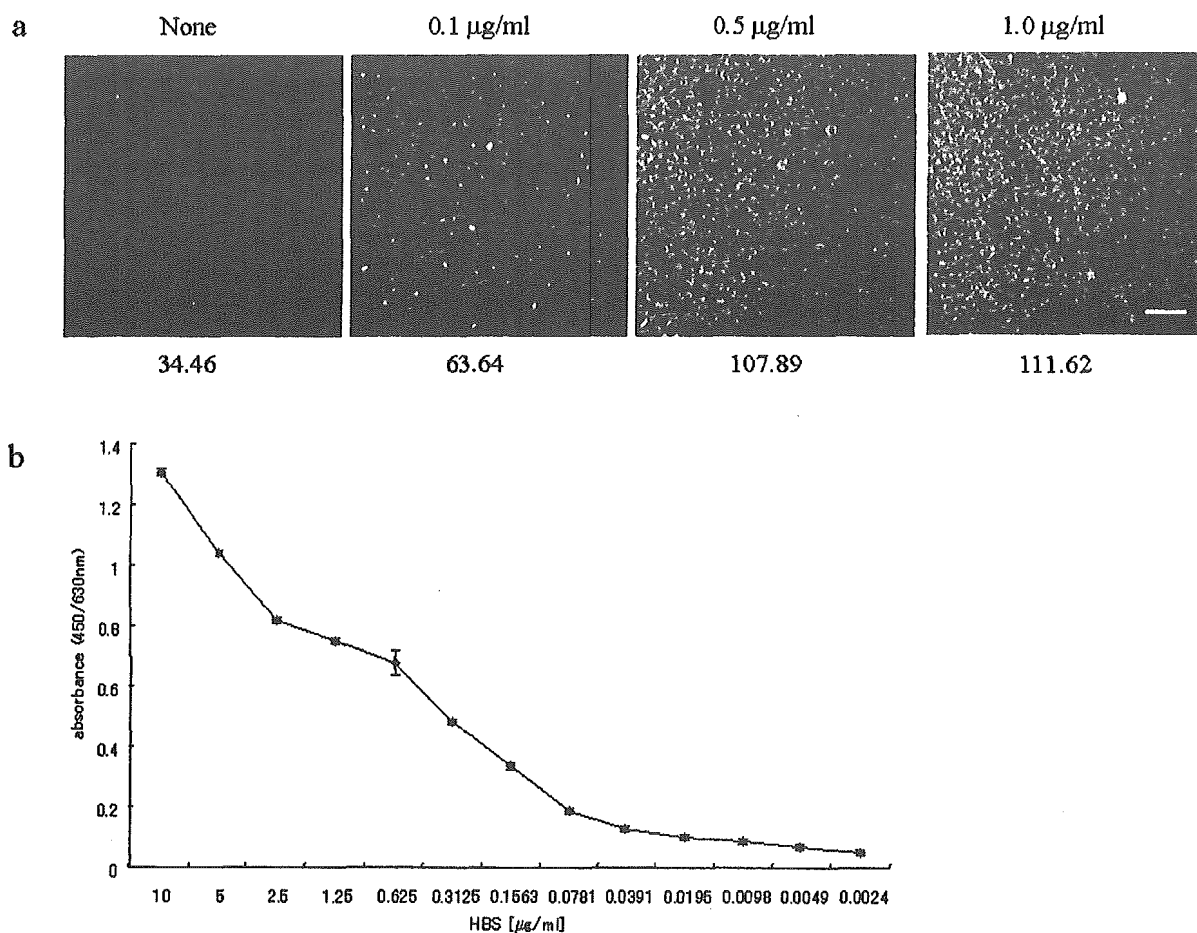


Fig. 6. Detection of viral antigen by TIRFM. (a) TIRFM imaging of human hepatitis virus antigen (HBs). HBs antigen was plated on the cover slip and detected by QD-conjugated anti-HBs antibody. Bars indicate 10  $\mu\text{m}$ . Detection sensitivity of HBs by ELISA was shown in (b). The data are presented as the mean  $\pm$  standard deviation of duplicated samples.

suitable for a multicolor and high-speed detection system.

It is extremely important to determine pathogenic bacteria rapidly and sensitively in biotechnology, medical diagnosis, and the current fight against bioterror-

ism. Current analysis techniques either lack ultrasensitivity or take a long time for analysis. In this method, the bioconjugated QDs provides an extremely high fluorescent signal for bioanalysis and can be easily incorporated with recognition of molecules. This system,

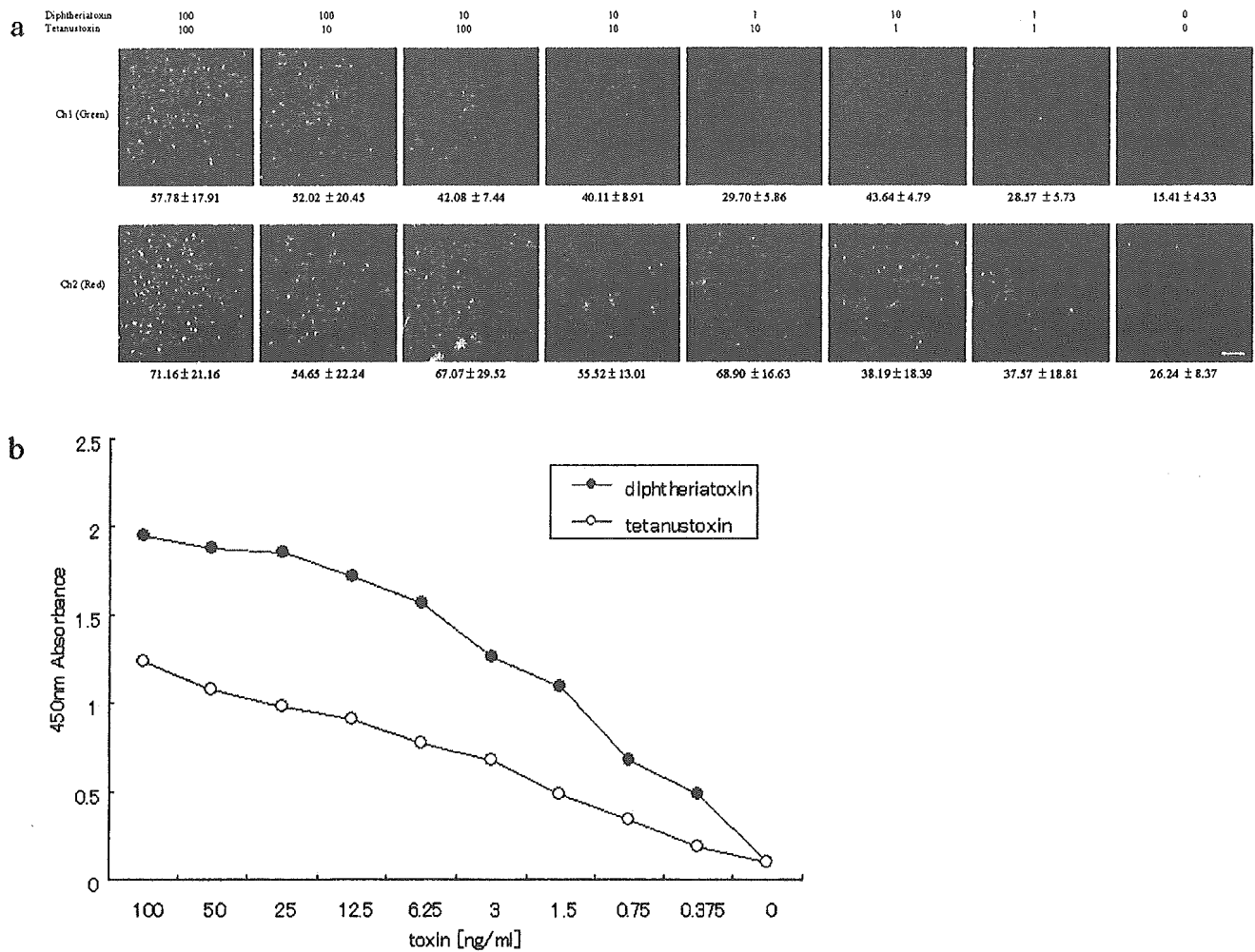


Fig. 7. Simultaneous detection of two bacterial toxins by TIRFM. (a) TIRFM imaging of diphtheria toxin and tetanus toxin. Mixture of two bacterial toxins were plated on the cover slip at indicated concentrations, and detected by anti-diphtheria toxin (QD520) and anti-tetanus toxin (QD640) antibodies. Bars indicate 10  $\mu$ m. (b) ELISA detection sensitivity of diphtheria and tetanus toxins. Anti-diphtheria toxin (human) or anti-tetanus toxin (rabbit) was added to 96-well plate. Toxins were detected by human or rabbit HRP-conjugated secondary antibodies. The data are presented as the mean  $\pm$  standard deviation of duplicated samples.

which was improved based on the recognition function of an antibody, has the same advantages as conventional immunoassay, which can measure specific target molecules with sufficient specificity. But unfortunately this system reflects the weak point of immunoassays. The sandwiching method is used commonly and widely in immunoassays; another epitope of target protein is recognized apart from the fixed antibody after catching the target protein. In general technique, detection was dependent on the secondary antibody that combines biotin or that were the specific antibody to the immunoglobulin of an immunized animal (e.g.; anti-human IgG), and then finally detected by the colorimetric substrate, the chemiluminescent reagents, or the fluorescence such as Alexa<sup>®</sup>fluor or CyChrome<sup>®</sup> dyes (26). Enhancement of assay performance has been achieved by several methods. Huang reported that simultaneous

detection of multiple proteins was demonstrated by an array-based enzyme-linked immunosorbent assay (ELISA) and enhanced chemiluminescence (ECL) (16), and Mattoussi et al., demonstrated by fluorescent probes by QDs (11). Almost all of the advanced assay use secondary antibody to enhance the sensitivity by using sandwiching method (29). However in a TIRFM detection system by the sandwiching method, quantum dot antibody is hard to be excited because secondary antibody exists far from the limit of distance on evanescent field.

This system is a novel immunological diagnostic methods, which can be expected to improve the high-throughput diagnosis that will be performed quickly and simply by this method compared with the conventional method. However, this method does not excel the conventional one in the sensitivity or certainty. As a



method of applying a system, the reaction system is integrated in the small cartridge and miniaturized to the portable size. For example, we expected that the system could make a significant contribution to judge the authenticity at high-speed and high sensitivity in the case of suspicions of the bioterrorism.

We are grateful to Dr. Shun-ichi Yamaya (Toyo Public Health College) for providing diphtheria toxin and anti-diphtheria toxin antibody (human). We thank Dr. Wayne Dawson (Chiba Institute of Technology, Chiba, Japan) for valuable help for proofreading, and Mr. Kazuyuki Ito and Mr. Kimiyoshi Arakawa (Department of Medical Ecology, Research Institute, IMCJ) for valuable help.

## References

- 1) Akerman, M.E., Chan, W.C., Laakkonen, P., Bhatia, S.N., and Ruoslahti, E. 2002. Nanocrystal targeting *in vivo*. *Proc. Natl. Acad. Sci. U.S.A.* **99**: 12617–12621.
- 2) Axelrod, D. 1989. Total internal reflection fluorescence microscopy. *Methods Cell Biol.* **30**: 245–270.
- 3) Bruchez, M., Jr., Moronne, M., Gin, P., Weiss, S., and Alivisatos, A.P. 1998. Semiconductor nanocrystals as fluorescent biological labels. *Science* **281**: 2013–2016.
- 4) Chan, W.C., and Nie, S. 1998. Quantum dot bioconjugates for ultrasensitive nonisotopic detection. *Science* **281**: 2016–2018.
- 5) Chan, W.C., Maxwell, D.J., Gao, X., Bailey, R.E., Han, M., and Nie, S. 2002. Luminescent quantum dots for multiplexed biological detection and imaging. *Curr. Opin. Biotech.* **13**: 40–46.
- 6) Dabboussi, B.O., Rodriguez-Viejo, J., Mikulec, F.V., Hein, J.R., Mattoussi, H., Ober, R., Jensen, K.F., and Bawendi, M.G. 1997. (CdSe)ZnS core-shell quantum dots; synthesis and characterization of size series of highly luminescent nanocrystallites. *J. Phys. Chem.* **101**: 9463–9475.
- 7) Dubertret, B., Skourides, P., Norris, D.J., Noireaux, V., Brivanlou, A.H., and Libchaber, A. 2002. *In vivo* imaging of quantum dots encapsulated in phospholipid micelles. *Science* **298**: 1759–1762.
- 8) Gao, X., Chan, W.C., and Nie, S. 2002. Quantum-dot nanocrystals for ultrasensitive biological labeling and multi-color optical encoding. *J. Biomed. Optics* **7**: 532–537.
- 9) Gao, X., Cui, Y., Levenson, R.M., Chung, L.W.K., and Nie, S. 2004. *In vivo* cancer targeting and imaging with semiconductor quantum dots. *Nat. Biotechnol.* **22**: 969–976.
- 10) Goldman, E.R., Anderson, G.P., Tran, P.T., Mattoussi, H., Charles, P.T., and Mauro, J.M. 2002. Conjugation of luminescent quantum dots with antibodies using an engineered adaptor protein to provide new reagents for fluoroimmunoassays. *Anal. Chem.* **74**: 841–847.
- 11) Goldman, E.R., Clapp, A.R., Anderson, G.P., Uyeda, H.T., Mauro, J.M., Medintz, I.L., and Mattoussi, H. 2004. Multiplexed toxin analysis using four colors of quantum dot fluororeagents. *Anal. Chem.* **76**: 684–688.
- 12) Hines, M.A., and Guyot-Sionnest, P. 1996. Synthesis and characterization of strongly luminescing ZnS-capped CdSe nanocrystals. *J. Phys. Chem.* **100**: 468–471.
- 13) Hoshino, A., Fujioka, K., Oku, T., Suga, M., Sasaki, Y.F., Ohta, T., Yasuhara, M., Suzuki, K., and Yamamoto, K. 2004. Physicochemical properties and cellular toxicity of nanocrystal quantum dots depend on their surface modification. *Nano Lett.* **4**: 2163–2169.
- 14) Hoshino, A., Fujioka, K., Oku, T., Suga, M., Nakamura, S., Yamaguchi, Y., Suzuki, K., Yasuhara, M., and Yamamoto, K. 2004. Quantum dots targeted to the assigned organelle in living cells. *Microbiol. Immunol.* **48**: 669–675.
- 15) Hoshino, A., Hanaki, K., Suzuki, K., Yamamoto, K. 2004. The applications T-lymphoma labeled with fluorescent quantum dots to cell trafficking markers in a mouse body. *Biochem. Biophys. Res. Commun.* **314**: 46–53.
- 16) Huang, R.P. 2001. Simultaneous detection of multiple proteins with an array-based enzyme-linked immunosorbent assay (ELISA) and enhanced chemiluminescence (ECL). *Clin. Chem. Lab. Med.* **39**: 209–214.
- 17) Ishii, D., Kinbara, K., Ishida, Y., Ishii, N., Okochi, M., Yohda, M., and Aida, T. 2003. Chaperonin-mediated stabilization and ATP-triggered release of semiconductor nanoparticles. *Nature* **423**: 628–632.
- 18) Jaiswal, J.K., Mattoussi, H., Mauro, J.M., and Simon, S.M. 2003. Long-term multiple color imaging of live cells using quantum dot bioconjugates. *Nat. Biotechnol.* **21**: 47–51.
- 19) Larson, D.R., Zipfel, W.R., Williams, R.M., Clark, S.W., Bruchez, M.P., Wise, F.W., and Webb, W.W. 2003. Water-soluble quantum dots for multiphoton fluorescence imaging *in vivo*. *Science* **300**: 1434–1436.
- 20) Mattoussi, H., Mauro, J.M., Goldman, E.R., Anderson, G.P., Sundar, V.C., Mikulec, F.V., and Bawendi, M.G. 2000. Self-assembly of CdSe-ZnS quantum dot bioconjugates using an engineered recombinant protein. *J. Am. Chem. Soc.* **122**: 12142–12150.
- 21) Rosenthal, S.J., Tomlinson, I., Adkins, E.M., Schroeter, S., Adams, S., Swafford, L., McBride, J., Wang, Y., DeFelice, L.J., and Blakely, R.D. 2002. Targeting cell surface receptors with ligand-conjugated nanocrystals. *J. Am. Chem. Soc.* **124**: 4586–4594.
- 22) Shubeita, G.T., Sekatskii, S.K., Dietler, G., Potapova, I., Mews, A., and Basch, T. 2003. Scanning near-field optical microscopy using semiconductor nanocrystals as a local fluorescence and fluorescence resonance energy transfer source. *J. Microsc.* **210**: 274–278.
- 23) Steyer, J.A., and Almers, W. 2001. A real-time view of life within 100 nm of the plasma membrane. *Nat. Rev. Mol. Cell Biol.* **2**: 268–275.
- 24) Toomre, D., and Manstein, D.J. 2001. Lighting up the cell surface with evanescent wave microscopy. *Trends Cell Biol.* **11**: 298–303.
- 25) Voura, E.B., Jaiswal, J.K., Mattoussi, H., and Simon, S.M. 2004. Tracking metastatic tumor cell extravasation with quantum dot nanocrystals and fluorescence emission-scanning microscopy. *Nat. Med.* **10**: 993–998.
- 26) Wiese, R., Belosludtsev, Y., Powdrill, T., Thompson, P., and Hogan, M. 2001. Simultaneous multianalyte ELISA performed on a microarray platform. *Clin. Chem.* **47**: 1451.
- 27) Wu, X., Liu, H., Liu, J., Haley, K.N., Treadway, J.A., Larson, J.P., Ge, N., Peale, F., and Bruchez, M.P. 2003.

- Immunofluorescent labeling of cancer marker Her2 and other cellular targets with semiconductor quantum dots. *Nat. Biotechnol.* **21**: 41–46.
- 28) Xu, H., Sha, M.Y., Wong, E.Y., Uphoff, J., Xu, Y., Treadway, J.A., Truong, A., O'Brien, E., Asquith, S., Stubbins, M., Spurr, N.K., Lai, E.H., and Mahoney, W. 2003. Multiplexed SNP genotyping using the Qbead system: a quantum dot-encoded microsphere-based assay. *Nucleic Acids Res.* **31**: 43.
- 29) Zhao, X., Hilliard, L.R., Mechery, S.J., Wang, Y., Bagwe, R.P., Jin, S., and Tan, W. 2004. A rapid bioassay for single bacterial cell quantitation using bioconjugated nanoparticles. *Proc. Natl. Acad. Sci. U.S.A.* **101**: 15027–15032.